ISSN: 0067-2904

Approximate Treatment for The MHD Peristaltic Transport of Jeffrey Fluid in Inclined Tapered Asymmetric Channel with Effects of Heat Transfer and Porous Medium

Mohammed R. Salman [1], Hayat A. Ali [2*]
[1] General Directorate of Education in the Holy Governorate of Karbala, Karbala, Iraq
[2]Department of Applied Science, University of Technology, Baghdad, Iraq

Received: 7/12/2019 Accepted: 29/1/2020

Abstract

In this paper, we discuss a fluid problem that has wide applications in biomechanics, polymer industries, and biofluids. We are concerned here with studying the combined effects of porous medium and heat transfer on MHD non-Newtonian Jeffery fluid which flows through a two dimensional asymmetric, inclined tapered channel. Base equations, represented by mass conservation, motion, energy and concentration conservation, were formulated first in a fixed frame and then transformed into a moving frame. By holding the assumptions of "long wavelength and low Reynolds number" these physical equations were simplified into differential equations. Approximate solutions for the velocity profile, stream function, and temperature profile were obtained using homotopy perturbation method. Finally, the graphical expressions and analysis for velocity curve, temperature distribution, heat transfer coefficient, and stream function, via the effects of important parameters that appear in the solution form, were given and examined. These results show a parabolic behavior for velocity distribution curve, the maximum value of which appears in the central part of the channel and reduces toward the lower and upper walls, due the impact of porosity parameter κ. While a decreasing behavior was observed via the effect of increasing Hartman number M (because of the existence of Lorentz force). Furthermore, the plots showed an increased function for Jeffrey fluid parameter λ_1 on the magnitude of the trapped bolus.

Keywords: Jeffrey fluid, Peristaltic transport, Porous medium, Asymmetric channel, Heat transfer.

المعالجة التقريبية لأنتقال التموجي لمائع جيفري المغناطيسي الهيدرودينميكي في قناة مدببة ومستدقة وغير متناضرة مع تأثير أنتقال الحرارة والوسط المسامي

محمد رزاق سلمان [1], حياةعادل علي [2*]
[1] المديرية العامة للتربية في محافظة كربلاء المقدسة, كربلاء, العراق
[2] قسم العلوم التطبيقية, الجامعة التكنلوجية, بغداد, العراق

الخلاصة

في هذا البحث نناقش مسالة مائع الغيرنيوتيني له تطبيقات واسعة في الميكانيكية الحيوية, كصناعة البوليمرات وصناعات الموائع الحيوية. نهتم هنا بدراسة الآثار المجتمعة للوسط المسامي ومبدأ الانتقال الحراري

*Email: mawb1967@gmail.com

لتدفق مائع (MHD) جيفري الغير النيوتيني من خلال قناة ثنائية الابعاد لامتناضرة مدببة ومائلة تقريبيا. المعادلات الاساسية المتمثلة بمعادلات حفظ الكتلة والحركة و حفظ الطاقة و حفظ التركيز, تمت صياغتها في البدء في إطار الاحداثيات الثابتة ومن ثم حولت الى نظام الموجة المتحركة، وبأخذ فرضية الطول الموجي الطويل، وعدد رينولدز القليل تم تبسيط هذه المعادلات الفيزيائية الى معادلات تفاضلية. تم الحصول على الحل التقريبي بالنسبة لملف السرعة ودالة التدفق ومنحني الحرارة باستخدام طريقة الاضطراب الهوموتوبي. وأخيرا تم اعطاء وأختبارالتعبيرات والتحليلات الصورية لكل من منحني السرعة، وتوزيع درجات الحرارة، ومعامل انتقال الحرارة، ودالة التدفق بالنسبة الى تأثير المعلمات المهمة التي تظهر في صيغة الحل.من خلال النتائج الصورية بينت سلوك القطع المكافيء لمنحني توزيع السرعة بالاضافة الى ذلك نلاحظ بان قيمتها العظمى تظهرفي الجزءالاوسط من القناة ومن ثم تتناقص باتجاه الجدار الاعلى والاسفل بسبب زيادة تأثير معلمة نفاذية الوسط . بينما نلاحظ السلوك التناقصي لمنحني متجه السرعة بسبب تأثيرتزايدعدد هارتمان (بسبب وجود قوة لورنز) . علاوة على ذلك هذه الرسوم اظهرت الصفة الناشئة لمعلمة مائع جيفري على الفقاعة المحصورة.

1. Introduction

Peristaltic transport occurs in many applications in our body and other processes in life such as urine flow through the ureter, food flow through the gastrointestinal tract, swallowing of food through esophagus, locomotion of worms, translocation of water in tall trees and in roller and finger pumps, nuclear industry, and heart lung machine [1]. This mechanism is identified as sinusoidal waves travelling along the length of the channel. Many researchers illustrated the peristaltic mechanism theoretically and experimentally to figure out its impact in different normal and pathological conditions [2, 3].

A non- Newtonian model in connection with peristalsis phenomenon has exploited the attention, since many fluids in physiology and industry are classified as non -Newtonian models. Blood, paints, shampoos, mud at low shear rate, among others, are examples of non- Newtonian models. A large amount of literature which connects peristalsis and non-Newtonian fluids is available recently [4-6]. Peristalsis with magneto-hydrodynamics interaction gathered much attention of many papers due to its applications in magnetic drug target, cancer diseases, blood flow, reduction of blood pressure, as well as MRI (Magnetic Resonance Imaging) and magneto therapy. Some recent investigations in relation to peristaltic flow of MHD fluid have been published [7, 8].

Besides that, the interaction of heat transfer analysis with peristalsis has a major impact in complex processes such as oxygenation, hemodialysis, tissues conduction, heat convection for blood flow from the pores, damage of undesirable cancer tissues, paper making, and food processing. Motivated by these facts, numerous studies have been also conducted [4, 9, 10].

This investigation addresses the electrically conducting Jeffrey fluid. This model of non-Newtonian fluid is a relatively simpler linear model that depends on time derivatives instead of convected derivatives. Moreover, it can indicate the changes of the rheology on the peristaltic flow even under the assumption of large wavelength, low Reynolds number, and small or large amplitude ratio. Lakshminarayana *et al*. [9] studied the slip and heat transfer impact on peristaltic flow of Jeffrey fluid in porous medium through a vertical asymmetric channel. Hayat *et al.* [10] examined the peristaltic flow of MHD Jeffrey fluid in a curved channel, where the Soret and Dufour impact and convective conditions were discussed. Reddy *et al.* [11] analyzed the impact of several forces on the peristaltic flow of Jeffrey nanofluid in an asymmetric channel. Vajravelu *et al*. [12] studied the peristaltic flow of Jeffery fluid in inclined asymmetric channel. More attempts which address Jeffery fluid under different situations can be found elsewhere [13, 14].

In this work, the heat transfer analyzed for peristaltic flow of Jeffrey fluid with slip boundary condition in an inclined tapered asymmetric porous channel is studied, taking into consideration the magnetic force. The governing equation of Jeffery fluid flow is formulated based on continuity, motion, and energy equations. The reduced system of differential equations is simplified by adopting the long wave length and low Reynolds number assumptions. Finally, the flow terms, velocity, temperature, heat transfer rate, and streamlines phenomenon are discussed graphically.

II. Problem Modeling

We take the peristaltic flows for incompressible MHD Jeffrey fluid in asymmetric inclined tapered channels with porous medium. The channel is inclined at an angle α to the horizontal axis with width $(d_1 + d_2)$. The electrically conducting non-Newtonian fluid is subjected to a magnetic force with flux $B = (0,0,\beta_0)$. Cartesian coordinate system is considered when the $\bar{X}$-axis is taken along the axial direction and the $\bar{Y}$-axis is normal to it. Furthermore, an infinite wave train moving along the walls of the channel with velocity c is considered, such that the asymmetry is induced in the channel when the non-uniform peristaltic wave train on the walls is assumed to have different amplitudes and phases. The geometry equation of the channel walls is given as

$$\bar{Y}_1 = \bar{H}_1(\bar{X},\bar{t}) = d_1 + \acute{m}\bar{X} + b_1 Sin\left(\frac{2\pi}{\lambda}(\bar{X} - c\bar{t})\right) \quad (1)$$

$$\bar{Y}_2 = \bar{H}_2(\bar{X},\bar{t}) = -d_2 - \acute{m}\bar{X} - b_2 Sin\left(\frac{2\pi}{\lambda}(\bar{X} - c\bar{t}) + \phi\right) \quad (2)$$

in which $\bar{Y}_1, \bar{Y}_2$ are the upper and lower walls, respectively, b_1, b_2 are the amplitudes of the lower and upper walls' waves, $\acute{m} \ll 1$ is the non- uniform parameter, $\phi \in [0,\pi]$ is the phase difference, and λ is the length of the wave. Consider that when $\phi = 0$ approaches the symmetric channel without phase waves and $\phi = \pi$ describes the in phase waves. In addition, $d_1, d_2, a, b,$ and ϕ satisfy the inequality in which the walls keep parallel.

$$b_1{}^2 + b_2{}^2 + b_1 b_2 Cos\phi \le (d_1 + d_2)^2 \quad \ldots(3)$$

$\bar{\tau}$ is the Cauchy stress tensor for Jeffrey fluid model, given by

$$\bar{\tau} = -\rho I + \bar{S},\ \bar{S} = \frac{\mu}{1+\lambda_1}\left(\dot{\gamma} + \lambda_2 \frac{d\dot{\gamma}}{dt}\right) \quad \ldots(4)$$

in which $\bar{S}$ is the extra stress tensor, ρ is the fluid density, I is the identity tensor, λ_1, λ_2 and $\dot{\gamma}$ are the ratios of relaxation to retardation times. The retardation time as well as the shear rate and dots over the quantities refer to time differentiation.

The governing equations of an incompressible fluid flow are given below, where the continuity equation has the form

$$\frac{\partial \bar{U}}{\partial \bar{X}} + \frac{\partial \bar{V}}{\partial \bar{Y}} = 0 \quad \ldots(5)$$

and the momentum equations are as follows

$$\rho\left(\frac{\partial \bar{U}}{\partial \bar{t}} + \bar{U}\frac{\partial \bar{U}}{\partial \bar{X}} + \bar{V}\frac{\partial \bar{U}}{\partial \bar{Y}}\right) = -\frac{\partial \bar{P}}{\partial \bar{X}} + \frac{\partial \bar{S}_{\bar{X}\bar{X}}}{\partial \bar{X}} + \frac{\partial \bar{S}_{\bar{X}\bar{Y}}}{\partial \bar{Y}} - \frac{\mu}{\kappa_0}\bar{U} - \sigma\beta_0^2\bar{U} + \rho g\beta(\bar{T} - T_0)Sin\alpha \quad \ldots(6)$$

and

$$\rho\left(\frac{\partial \bar{V}}{\partial \bar{t}} + \bar{U}\frac{\partial \bar{V}}{\partial \bar{X}} + \bar{V}\frac{\partial \bar{V}}{\partial \bar{Y}}\right) = -\frac{\partial \bar{P}}{\partial \bar{Y}} + \frac{\partial \bar{S}_{\bar{Y}\bar{X}}}{\partial \bar{X}} + \frac{\partial \bar{S}_{\bar{Y}\bar{Y}}}{\partial \bar{Y}} - \frac{\mu}{\kappa_0}\bar{V} - \sigma\beta_0^2\bar{V} + \rho g\beta(\bar{T} - T_0)Cos\alpha \quad \ldots(7)$$

Also, the energy equation has the form

$$\rho C_p\left(\frac{\partial \bar{T}}{\partial \bar{t}} + \bar{U}\frac{\partial \bar{T}}{\partial \bar{X}} + \bar{V}\frac{\partial \bar{T}}{\partial \bar{Y}}\right) = K\left(\frac{\partial^2 \bar{T}}{\partial \bar{X}^2} + \frac{\partial^2 \bar{T}}{\partial \bar{Y}^2}\right) + 2\mu\left(\left(\frac{\partial \bar{U}}{\partial \bar{X}}\right)^2 + \left(\frac{\partial \bar{V}}{\partial \bar{Y}}\right)^2\right) + \mu\left(\frac{\partial \bar{V}}{\partial \bar{X}} + \frac{\partial \bar{U}}{\partial \bar{Y}}\right) - \frac{\mu}{\kappa_0}\bar{U}^2, \quad \ldots(8)$$

where $\bar{U}, \bar{V}, \rho, \mu, g, \bar{T}, T_0, \bar{P}, \beta, C_p, K, \kappa_0, \sigma, \bar{X}, \overline{\text{and } Y}$ are the laboratory frame velocity components. The fluid density, the fluid dynamic viscosity coefficient, the gravity acceleration, the temperature field, the mean value of temperature, the pressure, the coefficient of thermal expansion, the constant pressure specific heat , the thermal conductivity, the permeability parameter, the electrical conductivity, directions of the fixed frame, and $S_{\bar{X}\bar{X}}, S_{\bar{X}\bar{Y}}, S_{\bar{Y}\bar{Y}}$ represent the components of extra stress tensor.

Now, the following transformation between a moving wave frame $(\bar{x},\bar{y})$ of velocity c and fixed frame $(\bar{X},\bar{Y})$ is given as

$$\bar{x} = \bar{X} - c\bar{t}, \bar{y} = \bar{Y}, \bar{u} = \bar{U} - c, \bar{v} = \bar{V},\ \bar{p}(\bar{x}) = \bar{p}(\bar{X},\bar{t}) \quad \ldots(9)$$

We will define the following non-dimensional quantities in order to reduce the number of extra parameters:

$$\left.\begin{array}{l} x=\frac{\bar{x}}{\lambda}\ , y=\frac{\bar{y}}{d_1}, u=\frac{\bar{u}}{c}\ , v=\frac{\bar{v}}{c\delta}\ , h_1=\frac{\bar{H}_1(X)}{d_1}\ , h_2=\frac{\bar{H}_2(X)}{d_1}, d=\frac{d_2}{d_1}, \delta=\frac{d_1}{\lambda}\ , a=\frac{b_1}{d_1}, \\ b=\frac{b_2}{d_1}, m=\frac{\acute{m}\lambda}{d_1}, p=\frac{{d_1}^2\bar{p}(X)}{\lambda\mu c}, Re=\frac{\rho c d_1}{\mu}, \kappa=\frac{\kappa_0}{{d_1}^2}, \theta=\frac{\bar{T}-T_0}{T_1-T_0}, Pr=\frac{\mu c\rho}{K}, s_{ij}=\frac{d_1}{\mu c}\bar{S}_{ij}, \\ M=\frac{\sigma{\beta_0}^2{d_1}^2}{\mu}, Ec=\frac{c^2}{C_p(T_1-T_0)}, N=EcPr, Gr=\frac{\beta g(T_1-T_0)d_1}{\upsilon c},\ {N_1}^2=\left(M^2+\frac{1}{\kappa}\right), \sigma=\frac{d_1}{\sqrt{\kappa_0}} \end{array}\right\} \quad \ldots(10)$$

where $Re, \delta, \sigma, Gr, Pr, \upsilon, Ec, \kappa, N, m$ are the number of Reynolds, the dimensionless number of waves, the permeability parameter, the Grashof number, the Prandtl number, the kinematic viscosity, the Eckert number, Darcy number, the parameter of perturbation, and the non-uniform parameter, respectively.

Then we defined the relationship between the stream function $\psi(x,y)$ and the two velocity components u, v by

$$u=\frac{\partial\psi}{\partial y},\ v=-\delta\frac{\partial\psi}{\partial x} \quad \ldots(11)$$

By making use of the dimensionless quantities of Eq. 10 into Eqs. 4-8, the mass equation is satisfied, and the non- dimensional momentum, energy equations, and the extra stress tensor components are derived below

$$Re\ \delta\left((u+1)\frac{\partial u}{\partial x}+v\frac{\partial u}{\partial y}\right)=-\frac{\partial p}{\partial x}+\delta\frac{\partial s_{xx}}{\partial x}+\frac{\partial s_{xy}}{\partial y}-\ {N_1}^2(u+1)+Gr\theta Sin\alpha \quad \ldots(12)$$

$$Re\ \delta^3\left((u+1)\frac{\partial v}{\partial x}+v\frac{\partial v}{\partial y}\right)=-\frac{\partial p}{\partial y}+\delta\frac{\partial s_{yy}}{\partial y}+\delta^2\frac{\partial s_{xy}}{\partial x}-\frac{1}{\kappa}\delta^2 v+\delta Gr\theta Cos\alpha \quad \ldots(13)$$

$$Re\ Pr\delta\left((u+1)\frac{\partial\theta}{\partial x}+v\frac{\partial\theta}{\partial y}\right)=\left(\delta^2\frac{\partial^2\theta}{\partial x^2}+\frac{\partial^2\theta}{\partial y^2}\right)+2\delta^2N\left(\left(\frac{\partial u}{\partial x}\right)^2+\delta\left(\frac{\partial v}{\partial y}\right)^2\right)$$
$$+N\left(\frac{\partial u}{\partial y}+\delta^2\frac{\partial v}{\partial x}\right)^2+\frac{N}{\kappa}(u+1)^2 \quad \ldots(14)$$

$$s_{xx}=\frac{2\delta}{1+\lambda_1}\left(1+\frac{c\delta\lambda_2}{a}\left(u\frac{\partial}{\partial x}+\frac{\upsilon}{\delta}\frac{\partial}{\partial y}\right)\right)\frac{\partial u}{\partial x} \quad \ldots(15)$$

where $s_{xy}=s_{yx}$, and

$$s_{xy}=\frac{1}{1+\lambda_1}\left(1+\frac{c\delta\lambda_2}{a}\left(u\frac{\partial}{\partial x}+\frac{\upsilon}{\delta}\frac{\partial}{\partial y}\right)\right)\left(\frac{\partial u}{\partial y}+\delta\frac{\partial v}{\partial x}\right) \quad (16)$$

$$s_{yy}=\frac{-2\delta}{1+\lambda_1}\left(1+\frac{c\delta\lambda_2}{a}\left(u\frac{\partial}{\partial x}+\frac{\upsilon}{\delta}\frac{\partial}{\partial y}\right)\right)\frac{\partial u}{\partial y} \quad \ldots(17)$$

By taking into consideration the low Reynolds number approximations, the long wavelength, and Eq.11, in Eqs. 12 – 17, we obtain that

$$\frac{\partial p}{\partial x}=\frac{1}{1+\lambda_1}\frac{\partial^2 u}{\partial y^2}-\ {N_1}^2(u+1)+Gr\theta Sin\alpha \quad \ldots(18)$$

$$\frac{\partial p}{\partial y}=0 \quad (19)$$

Eq. 19 indicates that the pressure vector p is independent of y coordinate and that it depends only on x coordinate.

$$\frac{\partial^2\theta}{\partial y^2}=-N\left(\frac{\partial u}{\partial y}\right)^2-\frac{N}{\kappa}(u+1)^2 \quad \ldots(20)$$

and

$$s_{xy}=\frac{1}{1+\lambda_1}\frac{\partial u}{\partial y} \quad \ldots(21)$$

While the dimensionless boundary conditions take the form

$$\left.\begin{aligned}\frac{\partial\psi}{\partial y} &= -1, \theta = 0 \quad at\ y = h_1(x,t) = 1 + m(x+t) + aSin(2\pi x)\\ \frac{\partial\psi}{\partial y} &= -1, \theta = 1 \quad at\ y = h_2(x,t) = -d - m(x+t) - bSin(2\pi x + \phi)\end{aligned}\right\} \quad \ldots(22)$$

III. Volumetric Flow Rate

The instantaneous volume flow in the fixed frame of coordinate $(\bar{X}, \bar{Y}, \bar{t})$ is given by

$$\bar{Q} = \int_{\bar{H}_1}^{\bar{H}_2} \bar{U}\,(\bar{X}, \bar{Y}, \bar{t})\, d\bar{Y} \quad \ldots(23)$$

in which $\bar{H}_1$ and $\bar{H}_2$ are depending on (x, t).

While in the moving frame, the flow becomes steady with respect to the reference $(\bar{x}, \bar{y})$. The expression of the volumetric flow rate becomes

$$q = \int_{h_1}^{h_2} \bar{u}\,(\bar{x}, \bar{y})\, d\bar{y} = \int_{h_1}^{h_2} c d_1 u\, dy \quad \ldots(24)$$

By substituting Eq.9 into Eq.23 and with Eq.24, the relation between the volumetric flow rates in the two frames is given by

$$\bar{Q} = \int_{\bar{H}_1}^{\bar{H}_2} (\bar{u} + c)\, d\bar{y} = \int_{h_1}^{h_2} (\bar{u} + c)\, d\bar{y} = q + c(\bar{H}_2 - \bar{H}_1) \quad \ldots(25)$$

The one periodic time- mean flow $\left(T = \frac{\lambda}{c}\right)$ for the peristaltic wave is given by

$$Q = \frac{1}{T}\int_0^T \bar{Q}\, d\bar{t} = \frac{1}{T}\int_0^T (q + c(h_2 - h_1) dy = q + 1 + d \quad \ldots(26)$$

The dimensionless time- mean flow Θ and F are introduced in the fixed and wave coordinates, respectively, as follows

$$\Theta = \frac{Q}{ca} \quad , \quad F = \frac{q}{ca}, \quad \ldots(27)$$

$$F = \int_{h_1}^{h_2} \frac{\partial\psi}{\partial y} = \psi(h_2) - \psi(h_1) \quad \ldots(28)$$

By employing Eq.28, we derive the following dimensionless relationship

$$\Theta = F - aSin(2\pi x) - bSin(2\pi x + \phi) \quad \ldots(29)$$

2. Solution of the problem

Eqs.18 and 20 are nonlinear differential equations which are impossible to determine an exact solution; Thus, we can use a perturbation technique. We expand u, θ, F and p for small values of perturbation parameter N as follows

$$\left.\begin{aligned} u &= u_0 + u_1 N + \cdots\\ \theta &= \theta_0 + \theta_1 N + \cdots\\ F &= F_0 + F_1 N + \cdots\\ p &= p_0 + p_1 N + \end{aligned}\right\} \quad \ldots(30)$$

By substituting Eq.30 into Eqs.18 and 20, we conclude that the following different order systems will be gained.

1. Zero order system

Consider the system of zero order

$$\frac{\partial p_0}{\partial x} = \frac{1}{1+\lambda_1}\frac{\partial^2 u_0}{\partial y^2} - {N_1}^2(u_0 + 1)Gr\theta_0 Sin\alpha, \quad \ldots(31)$$

By differentiating the above equation we get

$$\frac{1}{1+\lambda_1}\frac{\partial^3 u_0}{\partial y^3} - {N_1}^2\frac{\partial u_0}{\partial y} + Gr\frac{\partial\theta_0}{\partial y}Sin\alpha = 0, \quad \ldots(32)$$

$$\frac{\partial^2\theta_0}{\partial y^2} = 0, \quad \ldots(33)$$

associated with the following boundary conditions

$$\left.\begin{aligned} u_0 = -1 \ , \ \theta_0 = 0 \quad at\ y = h_1\\ u_0 = -1 \ , \ \theta_0 = 1 \quad at\ y = h_2\end{aligned}\right\} \quad \ldots(34)$$

By solving the above system, the closed form of zero order solution will be obtained as below

$$\theta_0 = C_1 + yC_2,$$

$u_0 = d_3 + \frac{\mathrm{Gr}y\mathrm{Sin}\alpha C_2}{N_1^2} - \frac{e^{-yN_1\sqrt{1+\lambda_1}}d_1}{N_1\sqrt{1+\lambda_1}} + \frac{e^{yN_1\sqrt{1+\lambda_1}}d_2}{N_1\sqrt{1+\lambda_1}},\ C_1 = \frac{h_1}{h_1-h_2}, C_2 = -\frac{1}{h_1-h_2},$

$d_1 = -((e^{h_1N_1\sqrt{1+\lambda_1}+h_2N_1\sqrt{1+\lambda_1}}\ GrSin\alpha C_2$
$(-e^{h_1N_1\sqrt{1+\lambda_1}} + e^{h_2N_1\sqrt{1+\lambda_1}} + \ h_1N_1\sqrt{1+\lambda_1} - h_2N_1\sqrt{1+\lambda_1}))/((e^{h_1N_1\sqrt{1+\lambda_1}} - e^{h_2N_1\sqrt{1+\lambda_1}} -$
$e^{2h_1N_1\sqrt{1+\lambda_1}+h_2N_1\sqrt{1+\lambda_1}} + e^{h_1N_1\sqrt{1+\lambda_1}+2h_2N_1\sqrt{1+\lambda_1}})N_1^2)),$

$d_2 =$
$(GrSin\alpha C_2(-e^{h_1N_1\sqrt{1+\lambda_1}} + e^{h_2N_1\sqrt{1+\lambda_1}} + e^{h_1N_1\sqrt{1+\lambda_1}+h_2N_1\sqrt{1+\lambda_1}}h_1N_1\sqrt{1+\lambda_1} -$
$e^{h_1N_1\sqrt{1+\lambda_1}+h_2N_1\sqrt{1+\lambda_1}}h_2N_1\sqrt{1+\lambda_1}))/((e^{h_1N_1\sqrt{1+\lambda_1}} - e^{h_2N_1\sqrt{1+\lambda_1}} - e^{2h_1N_1\sqrt{1+\lambda_1}+h_2N_1\sqrt{1+\lambda_1}} +$
$e^{h_1N_1\sqrt{1+\lambda_1}+2h_2N_1\sqrt{1+\lambda_1}})N_1^2)\ ,$

$d_3 = -((e^{2h_1N_1\sqrt{1+\lambda_1}}\mathrm{GrSin}\alpha C_2 - e^{2h_2N_1\sqrt{1+\lambda_1}}\mathrm{GrSin}\alpha C_2 - e^{h_1N_1\sqrt{1+\lambda_1}}GrSin\alpha C_2h_1N_1\sqrt{1+\lambda_1}/$
$((-e^{h_1N_1\sqrt{1+\lambda_1}} + e^{h_2N_1\sqrt{1+\lambda_1}} + e^{2h_1N_1\sqrt{1+\lambda_1}+h_2N_1\sqrt{1+\lambda_1}} - e^{h_1N_1\sqrt{1+\lambda_1}+2h_2N_1\sqrt{1+\lambda_1}})N_1^3\sqrt{1+\lambda_1})),$

2. First order system

The concluded first order system is given as

$\frac{\partial p_1}{\partial x} = \frac{1}{1+\lambda_1}\frac{\partial^2 u_1}{\partial y^2} - \ {N_1}^2u_1 + Gr\theta_1 Sin\alpha,$
…(35)

$\frac{1}{1+\lambda_1}\frac{\partial^3 u_1}{\partial y^3} - \ {N_1}^2\frac{\partial u_1}{\partial y} + Gr\frac{\partial \theta_1}{\partial y}Sin\alpha = 0,$ …(36)

$\frac{\partial^2 \theta_1}{\partial y^2} = -\left(\frac{\partial^2 u_0}{\partial y^2}\right)^2 - \frac{1}{k}(u_0+1)^2,$ (37)

associated with the following boundary conditions

$\left.\begin{array}{l} u_1 = 0\ ,\ \theta_1 = 0 \quad at\ y = h_1 \\ u_1 = 0\ ,\ \theta_1 = 0 \quad at\ y = h_2 \end{array}\right\}$ …(38)

The closed form for the solution are obtained, by applying Mathematica 10 program, as follows

$\theta_1 = d_4 + yd_5 + \frac{1}{12kN_1^6(1+\lambda_1)^2}(-Gr^2y^4Sin\alpha^2C_2^2N_1^2(1+\lambda_1)^2 - 4Gry^3Sin\alpha C_2(1+d_3)N_1^4(1+$
$\lambda_1)^2 - 3e^{-2yN_1\sqrt{1+\lambda_1}}d_1^2N_1^2(1+kN_1^2(1+\lambda_1)) - 3e^{2yN_1\sqrt{1+\lambda_1}}d_2^2N_1^2(1+kN_1^2(1+\lambda_1)) +$
$24e^{-yN_1\sqrt{1+\lambda_1}}d_1((1+d_3)N_1^3\sqrt{1+\lambda_1} + GrSin\alpha C_2 + yN_1\sqrt{1+\lambda_1} - kN_1^2(1+\lambda_1)))\ ,$

$u_1 =$
$s_3 - \frac{e^{-yN_1\sqrt{1+\lambda_1}}s_1}{N_1\sqrt{1+\lambda_1}} + \frac{e^{yN_1\sqrt{1+\lambda_1}}s_2}{N_1\sqrt{1+\lambda_1}} +$
$\frac{1}{24kN_1^9(1+\lambda_1)^2}(-1+Cos2\alpha+iSin2\alpha)\left(-ie^{-2yN_1\sqrt{1+\lambda_1}}GrCos\alpha d_1^2N_1^3 -\right.$
$\left.e^{-2yN_1\sqrt{1+\lambda_1}}GrSin\alpha d_1^2N_1^3\right)(1+kN_1^2+kN_1^2\lambda_1) +$
$\frac{1}{24kN_1^9(1+\lambda_1)^2}(-1+Cos2\alpha+iSin2\alpha)\left(-ie^{2yN_1\sqrt{1+\lambda_1}}GrCos\alpha d_2^2N_1^3 - e^{2yN_1\sqrt{1+\lambda_1}}GrSin\alpha d_2^2N_1^3\right)$

Where

$s_3 =$
$-\frac{1}{24kN_1^9(1+\lambda_1)^2}(-1+Cos2\alpha+iSin2\alpha)\left(-ie^{-2h_1N_1\sqrt{1+\lambda_1}}GrCos\alpha d_1^2N_1^3 -\right.$
$\left.e^{-2h_1N_1\sqrt{1+\lambda_1}}GrSin\alpha d_1^2N_1^3\right)(1+kN_1^2+kN_1^2\lambda_1) -$

$$\frac{1}{24kN_1^9(1+\lambda_1)^2}(-1+Cos2\alpha+iSin2\alpha)\left(-ie^{2h_1N_1\sqrt{1+\lambda_1}}GrCos\alpha d_2^2N_1^3-e^{2h_1N_1\sqrt{1+\lambda_1}}GrSin\alpha d_2^2N_1^3\right)(1+kN_1^2+kN_1^2\lambda_1)-\frac{1}{24kN_1^9(1+\lambda_1)^2}\left(-\frac{1}{4}iCos3\alpha h_1^4-\frac{1}{4}Sin3\alpha h_1^4\right),$$

$$d_4=$$

$$-\frac{1}{h_1-h_2}\left(-\frac{1}{12kN_1^6(1+\lambda_1)^2}h_2(-Gr^2Sin\alpha^2C_2^2h_1^4N_1^2(1+\lambda_1)^2-4GrSin\alpha C_2-24e^{h_2N_1\sqrt{1+\lambda_1}}d_2\left((1+d_3)N_1^3\sqrt{1+\lambda_1}+GrSin\alpha C_2\left(-2+h_2N_1\sqrt{1+\lambda_1}+kN_1^2(1+\lambda_1)\right)\right)\right)\right)$$

$$d_5=-((e^{-2h_1N_1\sqrt{1+\lambda_1}-2h_2N_1\sqrt{1+\lambda_1}}(-48e^{2h_1N_1\sqrt{1+\lambda_1}+h_2N_1\sqrt{1+\lambda_1}}\mathrm{GrSin}\alpha C_2d_1/(12k(h_1-h_2)N_1^6(1+\lambda_1)^2))$$

The values of coefficients(C_3,C_4,C_5,C_6) are large and non-constant. They are calculated by applying the boundary conditions in Eq.38 using Mathematica 10 programs.

3. Graphical Discussion

This part of the work explains the plotted outcomes of all the important parameters (e.g. parameter of permeability σ, the Grashof number Gr, the Hartman number, porosity parameter κ, the Jeffrey parameter λ_1, parameter of perturbation N, phase difference parameter ϕ, non-uniform parameter m) on the velocity distribution, temperature profile, heat transfer rate, and the streamline contours.

1. Velocity Profile

The velocity curve was drawn for fixed values of $\{x=0.1,t=0.1\}$ and the graphs show that the behavior of velocity distribution is parabolic in nature. Figure-1a detects the variation of $u(y)$ curve upon different values of Hartman number M. One can conclude that $u(y)$ values decreases against the enhancement of M magnitude. Two different reactions of the porosity parameter κ impact on $u(y)$ are seen, i.e. an increase on $u(y$)curve in the central part of the channel is observed for ascending values of κ, while a reduction function near the upper and lower walls are noticed (Figure-1b). The impact of Gershof number on velocity curve is plotted in Figure-2a. It is observed that the velocity curve grows up with the increase in the value of Gershof parameter. From Figure-2b, we conclude an increasing effect of Jeffrey parameter $\lambda_1$on the velocity axial. A descending behavior on the velocity profile is noticed due to the increase in the phase difference parameter ϕ (Figure-3a). In Fig.3b, the impact of the perturbation parameter N on $u(y)$ is illustrated, indicating an increase along the length of the channel.

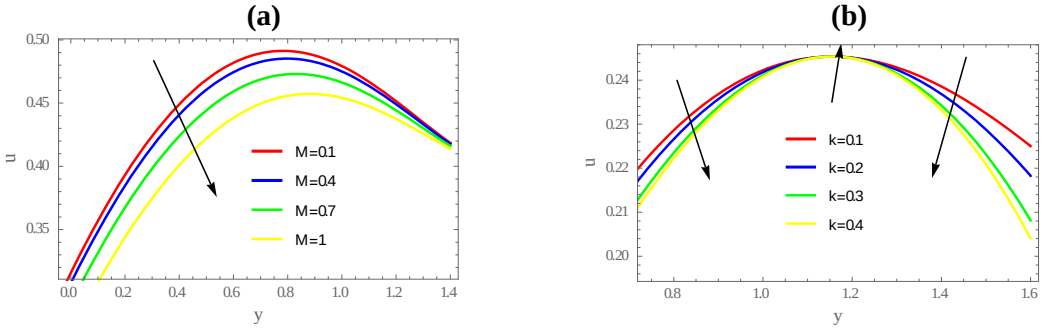

Figure 1- Velocity profile with various magnitudes of (a) Hartman number M, (b) Porosity parameter κ , for fixed values of parameters $\{\phi=\pi/10,\alpha=\pi/6,a=0.7,b=1,d=0.1,N=0.1,Gr=1,\Theta=0.2,m=0.2,\lambda_1=0.5\}$.

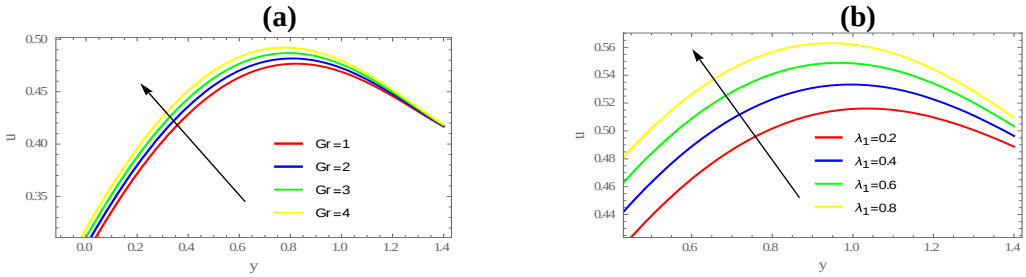

Figure 2- Velocity profile with various magnitudes of (a) Gershof number Gr, (b) Jeffrey parameterλ_1 , for fixed values of parameters $\{\phi = \pi/10\,, \alpha = \pi/6\,, a = 0.7, b = 1, d = 0.1, N = 0.1, \Theta = 0.2, m = 0.2, M = 0.1, \kappa = 0.2\}$.

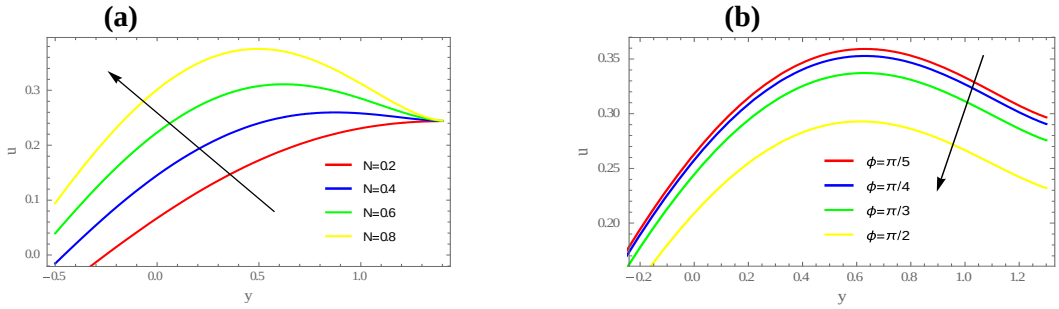

Figure 3- Velocity profile with various magnitudes of (a) phase difference parameter ϕ, (b) perturbation parameter N, for fixed values of parameters $\{\alpha = \pi/6\,, a = 0.7, b = 1, d = 0.1, Gr = 1, \Theta = 0.2, m = 0.2, \lambda_1 = 0.5, M = 0.1, \kappa = 0.2\}$.

2. Temperature Distribution

Figures 4-6 show the manner of the temperature distribution for various values of ($Gr, M, \kappa, N, \lambda_1$ and m). One can observe from these figures that $\theta(y)$ attains a maximum value in the central part of the channel. Figure-4a depicts that the increment of Gershof number tends the temperature curve $\theta(y)$ to increase. Figure-4b shows the reverse of the reaction of Hartman number on $\theta(y)$ profile. It is found that when the value of M rises the temperature distribution enlarges. When the magnitude of porosity parameter κ is high, a remarkable resistance in temperature curve is produced (Figure-5a). The behavior of the perturbation parameter N on temperature profile is sketched in Figure-5b, demonstrating that the enhancement in N causes an increase in $\theta(y)$ magnitude. Higher values of Jeffery parameter λ_1 cause an enhancement in the temperature profile (Figure-6a). Similar observations are made with ascending values of non-uniform parameter m against $\theta(y)$, i.e. the generation of more heat and hence the increase of $\theta(y)$ (Figure-6b).

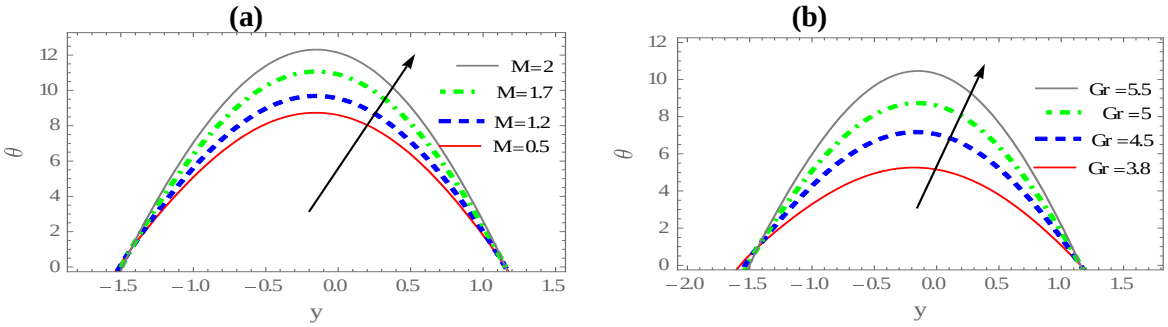

Figure 4- Temperature profile with various values of (a) Gershof number, (b) Hartman number , for fixed values of parameters $\{\alpha = \pi/6\,, a = 0.7, b = 1, d = 0.1, \text{“}N = 0.1\text{”}, \phi = \frac{\pi}{3}, \Theta = 0.2, \text{“}m = 0.2\text{”}, \lambda_1 = 0.5, \kappa = 0.2\}$.

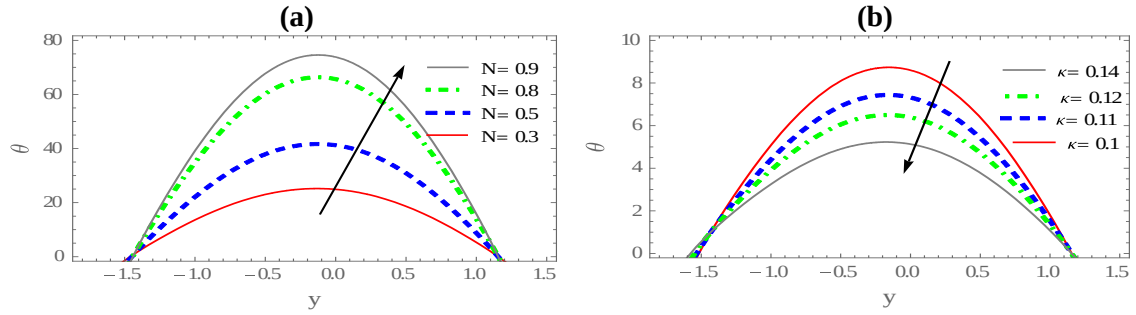

Figure 5- Temperature profile with various values of (a) Porosity parameter κ, (b) perturbation parameter N, for fixed values of parameters $\{\alpha = \pi/6, a = 0.7, b = 1, d = 0.1, \text{“}N = 0.1\text{”}, \phi = \frac{\pi}{3}, \Theta = 0.2, \text{“}m = 0.2\text{”}, \lambda_1 = 0.5, M = 0.1, Gr = 0.2\}$.

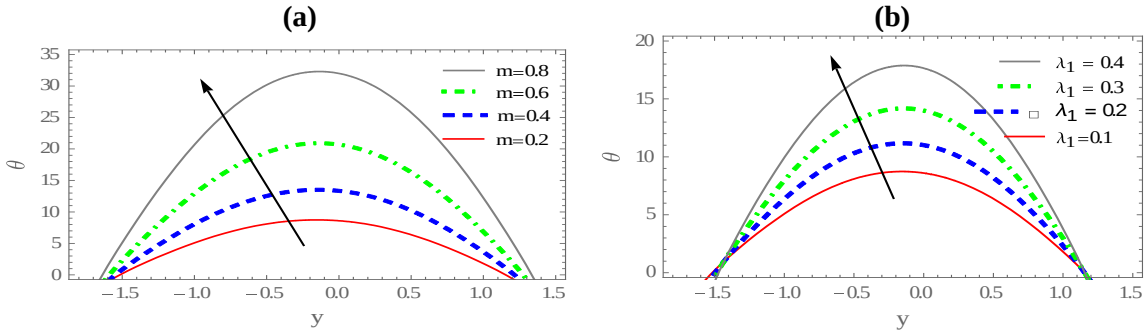

Figure 6- Temperature profile with various values of (a) Jeffery number λ_1, (b) non-uniform parameter m, for fixed values of parameters $\{\alpha = \pi/6, a = 0.7, b = 1, d = 0.1, \text{“}N = 0.1\text{”}, \phi = \frac{\pi}{3}, \Theta = 0.2, \kappa = 0.2, M = 0.1, Gr = 0.2\}$.

3. Heat transfer rate

Figures-(7-9) show the flow structure of heat transfer coefficient $Z(x)$ at the wall $y = h_2$, for various magnitudes of parameters (M, b, N, Gr, κ, m). We noticed that the heat transfer profile takes an oscillatory type. Figures- 7a, b and 8a, b display the effect of Hartman number, amplitude of upper wall b, perturbation parameter N, and Gershof number Gr on heat transfer $Z(x)$ profile. One can notice the mixed behavior for the heat transfer profile against ascending values of $M, b, N,$ and Gr along the length of the channel; i.e. the profile increases in the upper part of the x- axis and decreases downwards. Whereas a decreasing function above the x-axis and an increasing function below it are observed through the uplifting values of porosity parameter κ (Figure-9a). It is noticed that there is a considerable increment in heat transfer profile for higher values of non-uniform parameter m (Figure-9b).

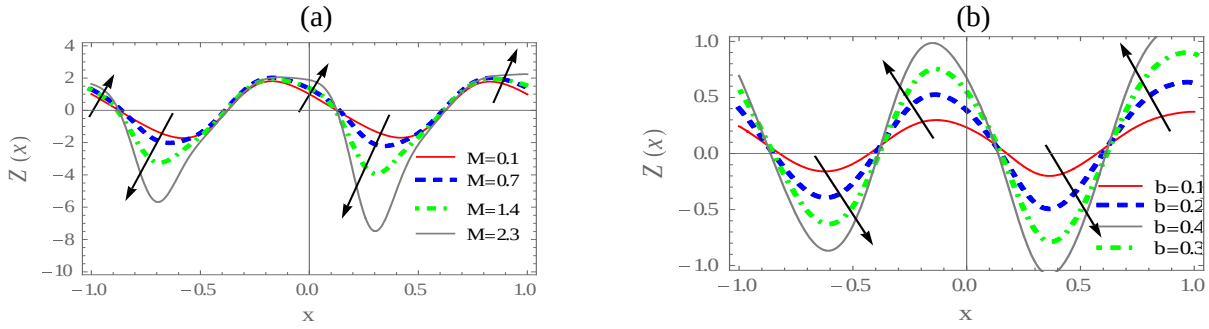

Figure 7- Heat transfer profile with various values of (a) Hartman number M, (b) Amplitude parameter of the upper wall, for fixed values of parameters $\{\alpha = \pi/6, a = 0.7, m = 0.1, d = 0.1, \text{“}N = 0.1\text{”}, \phi = \frac{\pi}{3}, \Theta = 0.2, \kappa = 0.2, \lambda_1 = 0.1, Gr = 0.2\}$.

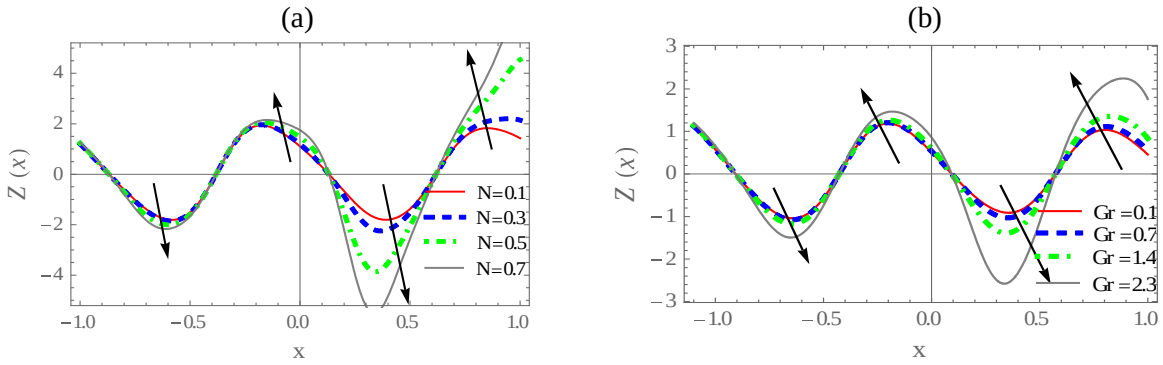

Figure 8- Heat transfer profile with various values of (a) Perturbation parameter N, (b) Gershof number Gr, for fixed values of parameters $\{\alpha = \pi/6\,, a = 0.7, \text{“}m = 0.1\text{”}, d = 0.1, M = 0.1, \text{“}\phi = \pi/3\text{”}, \Theta = 0.2, \kappa = 0.2, \lambda_1 = 0.1, b = 0.2\}$.

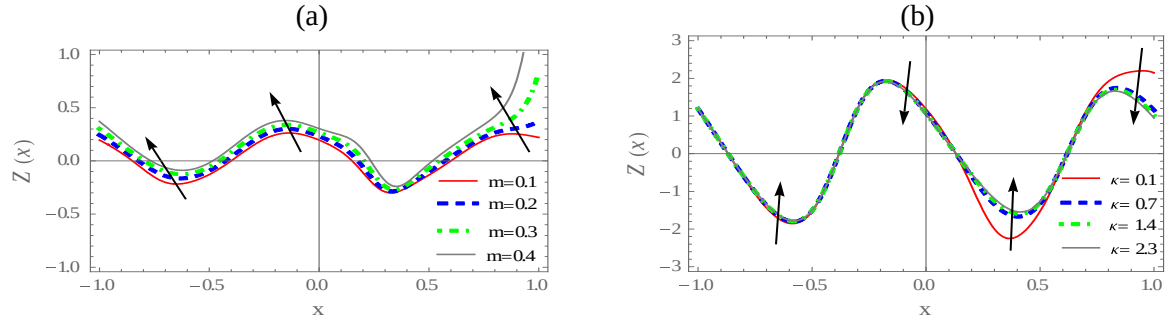

Figure 9- Heat transfer profile with various values of (a) Porosity parameter κ, (b) Non-uniform parameter m, for fixed values of parameters $\{\alpha = \pi/6\,, a = 0.7, N = 0.1, d = 0.1, M = 0.1, \phi = \pi/3\,, \Theta = 0.2, Gr = 0.2, \lambda_1 = 0.1, b = 0.2\}$.

4. Trapping Phenomena

The formation of internally circulating bolus that is enclosed by streamlines is known as trapping, which is moving along the peristaltic waves. Figures- 10-14 are presented to illustrate the behavior of different parameters on streamlines via Hartman number M, porosity parameter κ, Gershof number Gr, perturbation parameter N, and Jeffrey parameter λ_1. It can be deduced from Figure-10 that upon decreasing the effect of Hartman number on the flow, the size of the trapped bolus decreases while its number remains constant. The action of porosity parameter on the trapped bolus is recorded in Figure-11. The magnitude of the trapping bolus shrinks in size while higher number of bolus is created. It is noted from Figure-12 that the values of trapped bolus, as well as its number, are moderately enhanced . The ascending magnitude of perturbation parameter N causes an increase in both size and number of trapped bolus (Figure-13). The behavior of flow against the variation of Jeffrey parameter λ_1 is recorded in Figure-14. The plot shows that the increase in λ_1 values causes an enhancement in the magnitude of trapped bolus, while its number is reduced.

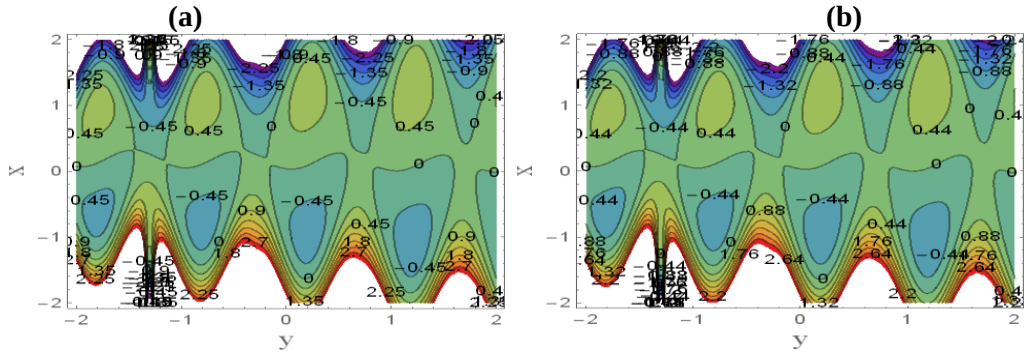

Figure 10- Stream function with various values of Hartman number $M = \{0.6, 0.9\}$ d for fixed values of parameters $\{\alpha = \pi/3\,, a = 0.4, m = 0.2, d = 0.6, Gr = 1, \phi = \frac{\pi}{6}, \Theta = 0.2, \kappa = 0.9, \lambda_1 = 0.5, b = 0.5, N = 0.1\}$.

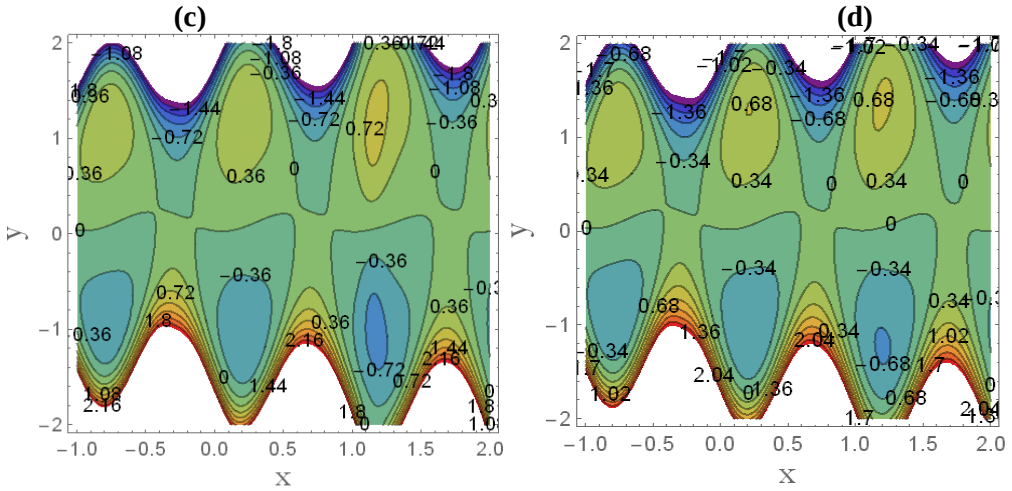

Figure 11- Stream function with various values of porosity parameter $\kappa = \{0.1, 0.2\}$ for fixed values of parameter $\{\alpha = \pi/3\,, a = 0.4, m = 0.2, d = 0.7, Gr = 1, \phi = \pi/8\,, \Theta = 0.2, M = 1, \lambda_1 = 0.2, b = 0.5, N = 0.1\}$.

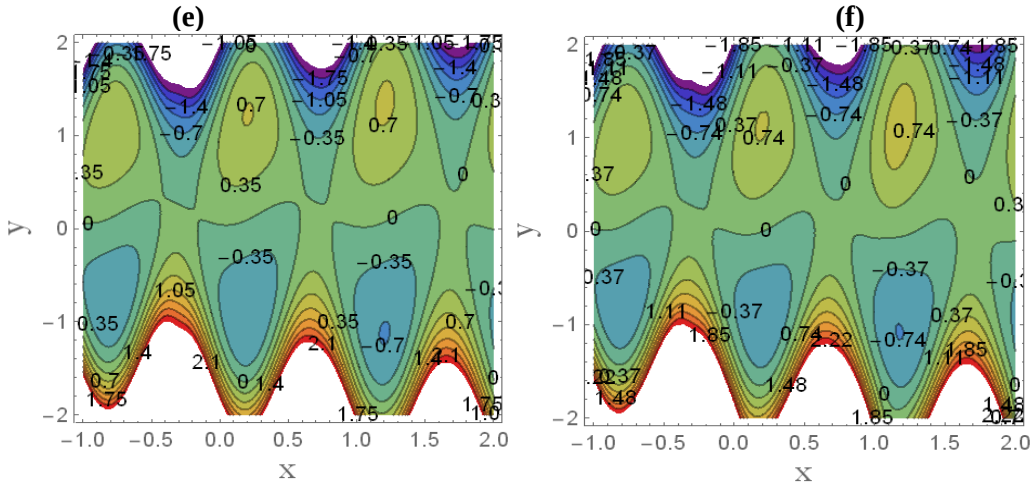

Figure 12- Stream function with various values of Gershof number $Gr = \{1, 3\}$ for fixed values of parameters $\{\alpha = \pi/3\,, a = 0.4, m = 0.2, d = 0.6, \kappa = 0.9, \phi = \pi/6\,, \Theta = 0.2, M = 0.8, \lambda_1 = 0.2, b = 0.5, N = 0.1\}$.

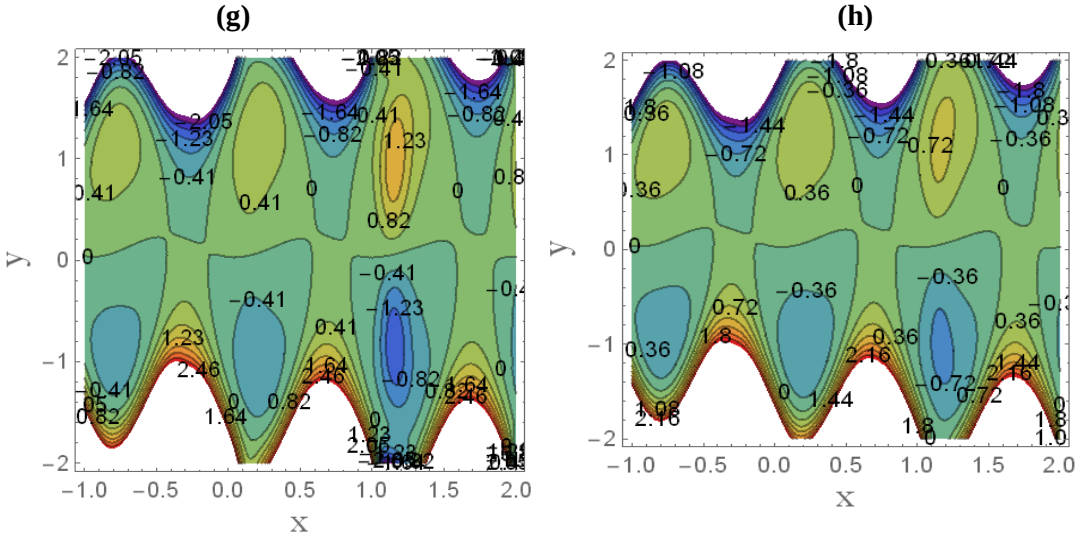

Figure 13- Stream function with various values of perturbation parameter $N = \{0.1, 0.3\}$ for fixed values of parameter $\{\alpha = \pi/3\,, a = 0.4, m = 0.2, d = 0.7, \kappa = 0.1, \phi = \pi/8\,, \Theta = 0.2, M = 1, \lambda_1 = 0.2, b = 0.5, Gr = 1\}$

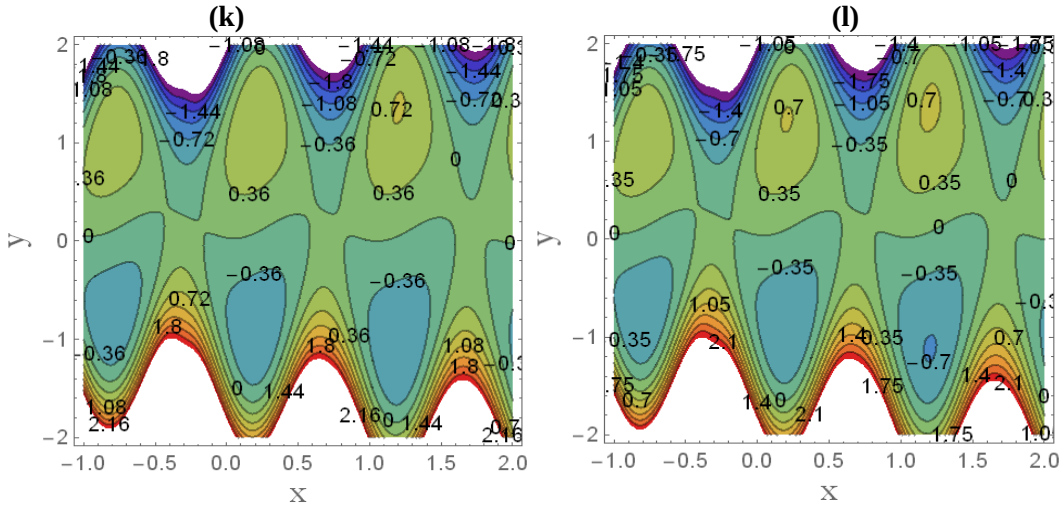

Figure 14- Stream function with various values of Jeffery number $\lambda_1 = \{0.1, 0.6\}$ for fixed values of parameter $\{\alpha = \pi/3, a = 0.4, m = 0.2, d = 0.6, \kappa = 0.1, \phi = \pi/6, \Theta = 0.2, M = 0.8, N = 0.1, b = 0.5, Gr = 1\}$.

4. Conclusions

In this investigation the effects of heat transfers and porous medium on the peristaltic transport of MHD Jeffrey fluid in an inclined tapered asymmetric channel are approximately determined using the perturbation technique, after simplifying the governing equation and energy equation depending on long wavelength assumption and small Renold number approximation. The significant outcomes of this study are listed below.

1. Velocity distribution has a parabolic behavior in nature, and it rises in the central part of channel and reduces due the impact of Hartman number, while an opposite behavior is seen via the effect of perturbation parameter. An increasing action in the central part of the channel and a reduction result near the walls are observed due to the increment of porosity parameter.
2. Gershof number and Jeffery number have the same effect of increasing the velocity profile.
3. Temperature distribution becomes higher in magnitude due to the effect of Hartman number, Gershof number, and perturbation parameter; however, it is diminished upon ascending values of porosity parameter.
4. The results of heat transfer rate show an oscillatory graphical picture due to contraction and expansion of peristaltic waves along the walls of the channel.
5. A mixed behavior for the absolute value of heat transfer is noticed across the peristaltic waves due to an increment in M, Gr, and κ, but an increasing effect for the non-uniform parameter m is depicted on $Z(x)$.
6. The size of the trapping bolus decreases upon an increment of Hartman number, while the bolus reduces in size and increases in number as the porosity parameter enhances.
7. The effects of Gr, N and λ_1 are opposite to one another, i.e. the magnitude of the bolus and number of circulations is increased with the increase in the magnitude of Gr and N, whereas it is decreased via the increase of Jeffery number values.

References

1. Ellahi. R., Hussain. F., Ishtiaq. F. and Hussain. A. **2019**. Peristaltic transport of Jeffrey fluid in a rectangular duct through a porous medium under the effect of partial slip: An application to upgrade industrial sieves/filters, *Pramana – Journal of physic*s, **93**(3). doi:10.1007/s12043-019-1781-8
2. Abbasi. F.M. and Shehzad. S.A. **2017**. Convective thermal and concentration transfer effects in hydromagnetic peristaltic transport with Ohmic heating. *Journal of Advanced Research*, **8**: 655-661
3. Asha. S. K. and Sunitha. G. **2018**. Mixed Convection Peristaltic flow of Eyring-Powell Nanofluid with Magnetic Field in a Non-Uniform Channel. *Journal of Applied Mathematics and Computation*, **2**(8): 332-344
4. Bintul Huda. A., Noreen Sher Akbar, Anwar Beg. O. and Yaqub Khan. M. **2017**. Dynamics of variable viscosity nanofluid flow with heat transfer in a flexible vertical tube under propagating waves. *Journal of Results in Physics*, **7**: 413-425
5. Farah. Aaa. Adnan, and Ahmed. M. Abdoulhadi. **2019**. Effect of inclined magnetic field on Peristaltic flow of Bingham plastic fluid in an inclined symmetric channel with slip conditions, *Iraqi Journal of Science*, **60**(7): 1551-1574.
6. Hayat. T., Anum Tanveera, and Alsaedi. A. **2016**. Numerical analysis of partial slip on peristalsis of MHD Jeffery nanofluid in curved channel with porous space, *Journal of Molecular Liquids*, doi:10.1016/j.molliq.2016.10.057.
7. Hayat. T., Maryiam Shafique, Anum Tanveer, and Alsaedi. A. **2016**. Magnetohydrodynamic effects on peristaltic flow of hyperbolic tangent nanofluid with slip conditions and Joule heating in an inclined channel, *International Journal of Heat and Mass Transfer*, **102**: 54-63
8. Mahmoud. Y. Abou-Zeid. **2018**. Homotopy Perturbation for Couple Stresses Effect on MHD Peristaltic Flow of a non-Newtonian Nanofluid, *Microsystem Technologies*, https:// doi.org/10.1007/s00542-018-3895-1
9. Lakshminarayana. P., Sreenadh. S., Sucharitha1.G. and Nandagopal. K. **2015**. Effect of slip and heat transfer on peristaltic transport of a Jeffrey fluid in a vertical asymmetric porous channel, *Advances in Applied Science Research*, **6**(2): 107-118
10. Tasawar. Hayat, Hina. Zahir, Anum. Tanveer and Ahmad. Alsaedi. **2017**. Soret and Dufour effects on MHD peristaltic transport of Jeffrey fluid in a curved channel with convective boundary conditions, PLOS ONE | DOI:10.1371/ journal pone.0164854 February 21.
11. Gnaneswara. Reddy. M. and Makinde. O.D. **2016**. Magnetohydrodynamic Peristaltic Transport of Jeffrey Nanofluid in an Asymmetric Channel, Reference: MOLLIQ 6357, DOI: doi:10.1016/j.molliq. 2016.09.080
12. Vajravelu. K., Sreenadh. S., Sucharitha. G. and Lakshminarayana. P. **2014**. Peristaltic transport of a conducting Jeffrey fluid in an inclined asymmetric channel, *International Journal of Biomathematics*, **7**(6):1450064 (25 pages)
13. Ellahi. R., Hussain. F., Ishtiaq. F. and Hussain. A. **2019**. Peristaltic transport of Jeffrey fluid in a rectangular duct through a porous medium under the effect of partial slip: An application to upgrade industrial sieves/filters, *Pramana – Journal of physic*s, **93**(3). doi:10.1007/s12043-019-1781-8.
14. Hayat. T., Khan. A.A., Farhat Bibi, Farooq. S. **2019**. Activation energy and non-Darcy resistance in magneto peristalsis of Jeffrey material, *Journal of Physics and Chemistry of Solids*, **129**: 155-161.